Rashba effect within the coherent scattering formalism

G. Feve,* W. D. Oliver, M. Aranzana,* and Y. Yamamoto†
Quantum Entanglement Project, ICORP, JST, E. L. Ginzton Laboratory, Stanford University, Stanford, California 94305
(Received 3 October 2001; revised manuscript received 25 June 2002; published 30 October 2002)

The influence of spin-orbit coupling in two-dimensional systems is investigated within the framework of the Landauer-Büttiker coherent scattering formalism. After a short review of the features of spin-orbit coupling in two-dimensional electron gases, we define the creation and annihilation operators for the stationary states of the Rashba spin-orbit coupling Hamiltonian and use them to calculate the current operator within the Landauer-Büttiker formalism. The current is expressed as it is in the standard spin-independent case, but with the spin label replaced by a new label, which we call the spin-orbit coupling label. The spin-orbit coupling effects can then be represented in a scattering matrix that relates the spin-orbit coupling stationary states in different leads. As an example, we calculate the scattering matrix in the case of a four-port beam splitter, and it is shown to mix states with different spin-orbit coupling labels in a manner that depends on the angle between the leads. A noise measurement after the collision of spin-polarized electrons at an electron beam splitter provides an experimental means to measure the Rashba parameter α. It is also shown that the degree of electron bunching in an entangled-electron collision experiment is reduced by the spin-orbit coupling according to the beam splitter lead angle.

DOI: 10.1103/PhysRevB.66.155328 PACS number(s): 72.10.Bg, 71.70.Ej, 73.50.Td

I. INTRODUCTION

Coherent electron transport through nanostructures in cryogenic two-dimensional electron gas systems is inherently a quantum mechanical phenomenon. Several experiments have demonstrated certain aspects of this quantum behavior, whether it relies directly on the wave nature of the electron and can be probed through a current or conductance measurement (e.g., quantized resistance in the quantum Hall effect,[1] conduction modes of a quantum point contact[2,3]) or on the particle nature and quantum statistics of the electrons or the electron source and can be probed through a noise measurement (e.g., Hanbury Brown and Twiss-type experiments,[4,5] electron collision,[6] observation of the fractional charge in the fractional quantum Hall effect.[7,8]) In addition, two-dimensional electron gases (2DEG's) could be used to study the fundamental nonlocal features of quantum mechanics through electron entanglement.[9–14]

These experiments can be successfully explained within the coherent scattering formalism,[15,16] a theoretical tool describing coherent and noninteracting particle transport. This formalism relies on spin-independent stationary states in the leads of the device and, therefore, describes spin-independent transport. Although it is possible to add a local spin-dependent effect directly in the scattering matrix, it is not possible in general to take into account spin effects occurring over the whole system. One potentially important spin effect occurring in the leads of the conductor is spin-orbit (SO) coupling. Any electric field in the reference frame of the laboratory generates a magnetic field in the moving electron reference frame, coupling the electron's orbital degrees of freedom with its spin. One can find several sources of electric fields in semiconductors. In three-dimensional crystals, the periodic crystal potential results in a bulk inversion asymmetry (the Dresselhaus effect[17]), which induces a spin splitting of the conduction band that is proportional to k^3 (k is the momentum of the conduction electron). In two-dimensional systems, the dominant term is due to structure inversion asymmetry (the Rashba effect[18]), resulting from the asymmetry of the in-plane confining potential and, more importantly, the heterojunction interface. This effect causes a spin splitting[19] proportional to k.

Recently, there has been a growing interest in electronic devices that rely on the spin properties of the electrons. These spin-dependent devices may be influenced by spin-orbit coupling effects or may even rely on them as, for example, in a coherent version of a spin-polarized field effect transistor.[20,21] Experiments involving Einstein-Podolsky-Rosen (EPR) type entangled-electron states may also be influenced by spin-orbit coupling.[9–14] With this motivation, we include spin-orbit coupling in the coherent scattering formalism.

II. SPIN-ORBIT COUPLING IN TWO-DIMENSIONAL ELECTRON GASES

Spin-orbit interactions are generally expressed in terms of the spin-orbit Hamiltonian[22] obtained through an expansion in v/c of the Dirac equation,

$$\hat{H}_I = \frac{\hbar}{(2m_0c)^2}\nabla V\cdot(\hat{\boldsymbol{\sigma}}\times\hat{\mathbf{p}}), \tag{1}$$

where m_0 is the free electron mass, $\hat{\mathbf{p}}$ is the momentum operator, $\hat{\boldsymbol{\sigma}}=(\hat{\sigma}_x,\hat{\sigma}_y,\hat{\sigma}_z)$ are the Pauli spin matrices, V is the electromagnetic scalar potential, and ∇ is the gradient operator, so that $-\nabla V$ is the electric field. According to Eq. (1), electron transport in the presence of an electric field results in a spin-orbit energy due to the coupling of the electron spin and orbital degrees of freedom through the $\hat{\boldsymbol{\sigma}}\times\hat{\mathbf{p}}$ term. Here, we will neglect the bulk inversion asymmetry (Dresselhaus effect) and consider only the the structure inversion asymmetry (Rashba effect), as the latter can dominate in the two-dimensional heterostructures of interest in this paper.[23–25] Let z be the direction of confinement, perpendicular to the

plane of motion. Originally, the asymmetry of the confining potential along the z direction was considered to be the source of a nonzero average electric field along the z axis, resulting in the Rashba spin-orbit coupling.[26] However, this mechanism underestimates the strength of the spin-orbit coupling, because the average electric field for the confined bound state in the quantum well is essentially zero[27] and only nonzero to the extent that the effective masses in the materials that define the confining potential are different. Rather, it has been shown through, for example, $\mathbf{k}\cdot\mathbf{p}$ models[28–31] that the dominant structure inversion asymmetry mechanism is related to the differing band discontinuities at the heterostructure quantum well interfaces for the conduction bands considered in the $\mathbf{k}\cdot\mathbf{p}$ model. In addition, these models show that the spin-orbit coupling energy is not necessarily proportional to $-\nabla V$ across the entire well.[31] Elsewhere, the particular role of an externally applied gate voltage to the tuning of the Rashba spin-orbit coupling strength and its modification of the interfacial electric field is also emphasized.[32–38] These various spin-orbit coupling mechanisms can be incorporated using the following model Hamiltonian [rather than Eq. (1)] for the structure inversion asymmetry we consider in this paper:

$$\hat{H}_{\mathrm{SO}}=\frac{\alpha}{\hbar}(\hat{\sigma}\times\hat{p})_z=i\alpha\left(\hat{\sigma}_y\frac{\partial}{\partial_x}-\hat{\sigma}_x\frac{\partial}{\partial_y}\right), \tag{2}$$

where α is the Rashba parameter, which characterizes the aggregate strength of the various spin-orbit coupling mechanisms. It takes values in the range $1-10\times10^{-10}$ eV cm for a large variety of systems [for example, $\mathrm{In}_x\mathrm{Ga}_{1-x}\mathrm{As}/\mathrm{In}_y\mathrm{Al}_{1-y}\mathrm{As}$ (Refs. 23 and 32), InAs/AlSb (Ref. 34), InAs/GaSb (Ref. 25), and $\mathrm{GaAs}/\mathrm{Al}_x\mathrm{Ga}_{1-x}\mathrm{As}$ (Ref. 39)] depending on the shape of the confining well. To simplify the presentation, we consider α to be independent of the in-plane momentum.

Using the standard effective mass approximation, we can deduce the system Hamiltonian as the free particle Hamiltonian plus the spin-orbit coupling Hamiltonian

$$\hat{H}=\frac{\hat{p}_x^2+\hat{p}_y^2}{2m}-\frac{\alpha}{\hbar}(\hat{\sigma}_y\hat{p}_x-\hat{\sigma}_x\hat{p}_y), \tag{3}$$

where m is taken to be the effective mass. Since the operators $\hat{p}_x$ and $\hat{p}_y$ commute with $\hat{H}$, we can search for eigenstates of the form

$$|\psi\rangle=e^{i(k_xx+k_yy)}[c_\uparrow|\uparrow\rangle+c_\downarrow|\downarrow\rangle], \tag{4}$$

where $|\uparrow\rangle$ and $|\downarrow\rangle$ label the up and down states of the z component of the spin. We can diagonalize the Hamiltonian

$$\hat{H}=\begin{pmatrix}\dfrac{\hbar^2k^2}{2m} & \alpha k_y+i\alpha k_x\\ \alpha k_y-i\alpha k_x & \dfrac{\hbar^2k^2}{2m}\end{pmatrix} \tag{5}$$

in this spin subspace. The eigenvalues are $E_\pm(k)=\hbar k^2/2m\pm\alpha k$, and the associated eigenfunctions are

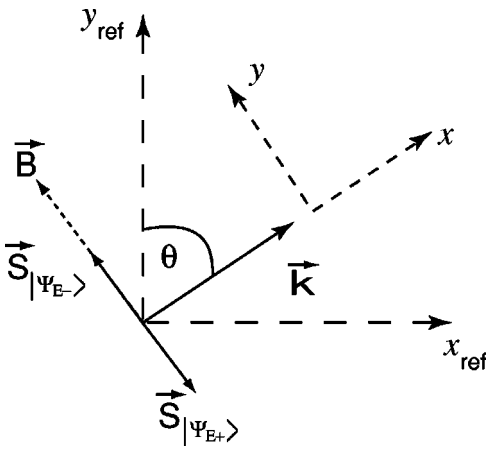

FIG. 1. Direction of the spin for the $|\Psi_{E_\pm}\rangle$ states. An electron with wave vector $\mathbf{k}$ feels a virtual field $\mathbf{B}(\mathbf{k},\alpha)$ perpendicular to $\mathbf{k}$. The spin direction $\mathbf{S}$ is aligned and antialigned to this field. The axes x_{ref} and y_{ref} designate a fixed reference frame. The axis x_γ is parallel to the momentum $\mathbf{k}$, which makes an angle θ_γ with the y_{ref} axis. In the extension to one-dimensional leads, γ will label the lead and $\mathbf{k}$ will be the longitudinal momentum.

$$|\Psi_{E_+}\rangle=\frac{e^{i(k_xx+k_yy)}}{\sqrt{2}}[e^{i\theta_\gamma/2}|\uparrow\rangle+e^{-i\theta_\gamma/2}|\downarrow\rangle], \tag{6}$$

$$|\Psi_{E_-}\rangle=\frac{e^{i(k_xx+k_yy)}}{\sqrt{2}}[e^{i\theta_\gamma/2}|\uparrow\rangle-e^{-i\theta_\gamma/2}|\downarrow\rangle], \tag{7}$$

where θ_γ is the angle between the in-plane momentum $\mathbf{k}$ and the axis y_{ref} of the reference laboratory frame (see Fig. 1). We have introduced the γ coordinate system in anticipation of a multilead device in which lead γ will have a particular orientation with respect to the reference laboratory frame.

The electrons feel a virtual, in-plane magnetic field in a direction perpendicular to $\mathbf{k}$. The spins of the stationary states are aligned and antialigned to this field (see Fig. 1), so that $\angle(\mathbf{k},\mathbf{S}_{|\Psi_{E_-}\rangle})=\pi/2$ and $\angle(\mathbf{k},\mathbf{S}_{|\Psi_{E_+}\rangle})=-\pi/2$, where $\angle(\mathbf{k},\mathbf{S}_{|E_-\rangle})$ is the angle between $\mathbf{k}$ and the spin $\mathbf{S}$ in the state $|\Psi_{E_-}\rangle$. The amplitude of the magnetic field depends on the velocity of the electron and vanishes for $k=0$, preventing a possible spin polarization in the system. The lack of spontaneous spin polarization is a reflection of the time-reversal invariance of the model Hamiltonian[21] in Eq. (2). The spin-orbit splitting is usually small compared to the kinetic energy of the electrons ($0.15\ \mathrm{meV}\leqslant\alpha k_F\leqslant1.5\ \mathrm{meV}$ for $E_F=14$ meV).

Following Ref. 15, we will introduce a transverse confinement in the leads of the conductor, allowing us to address the longitudinal transport modes for each transverse mode. Focusing on one lead γ, we make two simplifying assumptions. First, we consider only a single-independent transverse mode. Second, we neglect the 1D SO coupling effect that this transverse confining potential could create, since, to our knowledge, there is no experimental verification of this effect, and it is estimated to be much smaller than the Rashba effect.[40] Within these approximations, we can use our previ-

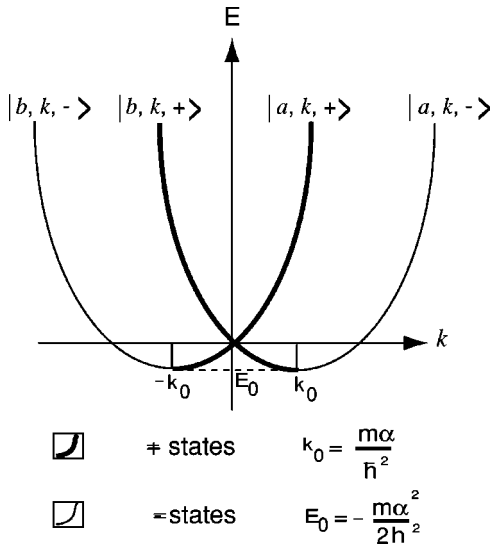

FIG. 2. Energy dispersion diagram with SO coupling. The $-\eta_\sigma k_0 \leqslant k < \infty$ range (a states) is defined in Eq. (8). The $-\infty < k < \eta_\sigma k_0$ range (b states) is then deduced by mirror symmetry.

ous analysis to deduce the eigenstates and the associated energy dispersion diagram (see Fig. 2), with k lying in the direction x_γ of the lead and making an angle θ_γ with the $y_{\rm ref}$ axis (see Figs. 1 and 3). We will now introduce three labels for the eigenstates that will prove useful in writing the creation and annihilation operators of these states: (1) ϵ labels the direction of propagation from the sign of the group velocity v_g: $\epsilon \equiv a$ if $v_g > 0$, $\epsilon \equiv b$ otherwise; (2) k labels the longitudinal mode wave vector along the x_γ axis; and (3) $\sigma \equiv \pm$ is called the SO coupling label; it designates the + and − branches of the energy dispersion diagram (as illustrated in Fig. 2) and, thereby, the spin direction for the SO states (see Figs. 3 and 4). Using these labels, we find the following eigenstates and eigenvalues of the system from Eqs. (6) and (7):

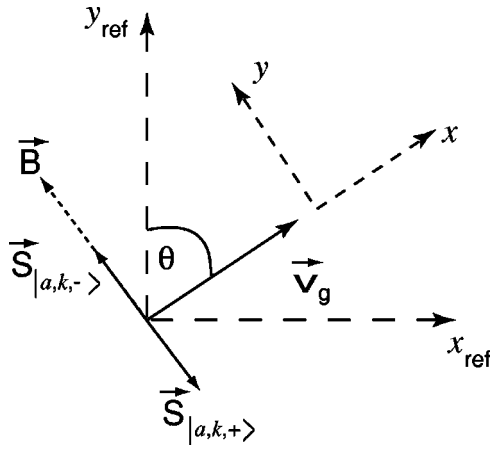

FIG. 3. Direction of the spin for the $|a,k,\pm\rangle$ states. The axes $x_{\rm ref}$ and $y_{\rm ref}$ designate a fixed reference frame. The axis x_γ is parallel to the momentum $\mathbf{k}$, which makes an angle θ_γ with the $y_{\rm ref}$ axis. In the extension to one-dimensional leads, γ will label the lead and $\mathbf{k}$ will be the longitudinal momentum.

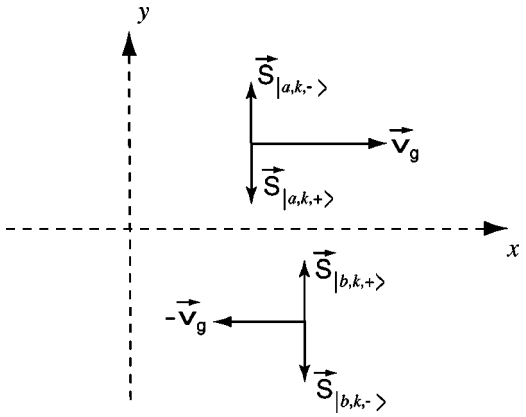

FIG. 4. Direction of the spin of χ^ϵ_σ. For notational convenience, the lead direction x_γ is aligned with the reference laboratory frame $x_{\rm ref}$ in Sec. III by moving the SO coupling angular dependence of lead γ into the scattering matrix.

$$|\epsilon,k,\sigma\rangle = \Phi(y_\gamma)\frac{e^{i\eta_\epsilon k x_\gamma}}{\sqrt{2}}[e^{i\theta_\gamma/2}|\uparrow\rangle + \eta_\epsilon\eta_\sigma e^{-i\theta_\gamma/2}|\downarrow\rangle],$$

$$E = \frac{\hbar^2 k^2}{2m} + \eta_\sigma \alpha k, \quad -\eta_\sigma k_0 \leqslant k < \infty, \tag{8}$$

where $\eta_\epsilon = +1$ (-1) corresponds to $\epsilon = a$ (b), and $\eta_\sigma = \pm 1$ corresponds to $\sigma = \pm$. Here $\Phi(y_\gamma)$ is the normalized transverse wave function for the transverse mode under consideration. By convention, k is only taken in the range $-\eta_\sigma k_0 \leqslant k < \infty$ for both the a and b states. The remaining eigenvalues in Fig. 2 can be deduced by mirror symmetry. We use $\eta_\epsilon = \pm 1$ to parametrize explicitly the appropriate wave vector range for the ϵ propagation direction in the eigenstate phase factor $e^{i\eta_\epsilon k x_\gamma}$. This convention allows us to track the propagation direction throughout the calculation.

We also notice in Fig. 2 that, for a given energy, the corresponding $|\epsilon,k,\pm\rangle$ states do not have the same wave vector,

$$\Delta k \equiv |k(\epsilon,E,+) - k(\epsilon,E,-)| = 2k_0 = \frac{2m\alpha}{\hbar^2}. \tag{9}$$

The $|\epsilon,k,\pm\rangle$ states have their spin perpendicular to the direction of propagation $\mathbf{v}_g$ and in opposite directions, such that $\angle(\mathbf{v}_g, \mathbf{S}_{|\epsilon,k,-\rangle}) = \pi/2$ and $\angle(\mathbf{v}_g, \mathbf{S}_{|\epsilon,k,+\rangle}) = -\pi/2$ (see Figs. 3 and 4). It is important to notice that the spin directions for the $|\epsilon,k,\pm\rangle$ states do not necessarily coincide with those of the $|\Psi_{E_\pm}\rangle$ states. The spin direction for the $|\epsilon,k,\pm\rangle$ states is determined by $\mathbf{v}_g$, while the spin direction for the $|\Psi_{E_\pm}\rangle$ states is determined by $\mathbf{k}$. The definition of spin direction is only consistent for states that share the same direction for both the longitudinal momentum $\mathbf{k}$ and the group velocity $\mathbf{v}_g$. For example, this is the case illustrated in Figs. 1 and 3. However, from the dispersion relation in Fig. 2, it is clear that there also exist energies for which positive (negative) k corresponds to negative (positive) v_g, and this means that the definitions of the spin direction are inconsistent for these energies. We choose here to link the direction

of the spin to $\mathbf{v}_g$ (rather than $\mathbf{k}$) through the label $\sigma=\pm$ (rather than $E_\pm$), because it is the group velocity that determines the direction of the current. In the absence of SO coupling, no differentiation between $\mathbf{v}_g$ and $\mathbf{k}$ is necessary, because they always share the same direction.

III. SPIN-ORBIT COUPLING AND THE COHERENT SCATTERING FORMALISM

The Landauer-Büttiker coherent scattering formalism relies on a second-quantization formulation of quantum mechanics. The current is expressed as a function of the field operator, which is expanded in the basis of the scattering states using the operators that create and destroy electrons in the leads of the conductor. A scattering state is a coherent sum of an incident wave in one lead and the outgoing waves it generates in all leads. The amplitude of each outgoing wave is given by the scattering matrix *S*, whose elements depend on the properties of the scatterer. As our final goal is to study the fluctuations of the current, it is important to find a simple way to express the time dependence of the current operator. In our rederivation of the coherent scattering formalism, we will follow the same approach as in Ref. 15, while introducing two important changes: (1) we will derive an expression for the current operator that includes a new contribution due to the spin-orbit coupling; (2) we will expand the field operator in the new stationary basis of the SO coupling Hamiltonian.

A. Calculation of the current operator

To find the current operator, we begin with the single-particle Schrödinger equation and the Hamiltonian in Eq. (5),

$$i\hbar\frac{\partial\Psi}{\partial t}=-\frac{\hbar^2}{2m}\left(\frac{\partial\Psi}{\partial x^2}+\frac{\partial\Psi}{\partial y^2}\right)+i\alpha\left(\sigma_y\frac{\partial\Psi}{\partial x}-\sigma_x\frac{\partial\Psi}{\partial y}\right), \tag{10}$$

where Ψ is a two-component spinor. The current operator $\hat{\mathbf{j}}$ can be inferred from the conservation of charge equation

$$\frac{\partial}{\partial t}[e\Psi^\dagger\Psi]+\boldsymbol{\nabla}\cdot\mathbf{j}=0,$$

using Eq. (10) and its adjoint:

$$j_x=\frac{e\hbar}{2mi}\left[\Psi^\dagger\frac{\partial\Psi}{\partial x}-\frac{\partial\Psi^\dagger}{\partial x}\Psi\right]-\frac{e\alpha}{\hbar}\Psi^\dagger\sigma_y\Psi, \tag{11}$$

$$j_y=\frac{e\hbar}{2mi}\left[\Psi^\dagger\frac{\partial\Psi}{\partial y}-\frac{\partial\Psi^\dagger}{\partial y}\Psi\right]+\frac{e\alpha}{\hbar}\Psi^\dagger\sigma_x\Psi. \tag{12}$$

We can identify the usual kinetic term of the current density

$$\mathbf{j}_{\mathrm{K}}=\frac{e\hbar}{2mi}[\Psi^\dagger\nabla\Psi-\nabla\Psi^\dagger\Psi]. \tag{13}$$

SO coupling adds a new contribution proportional to α that we call the SO coupling current density $\mathbf{j}_{\mathrm{SO}}$:

$$\mathbf{j}_{\mathrm{SO}}=-\frac{e\alpha}{\hbar}\Psi^\dagger\sigma_y\Psi\mathbf{u}_x+\frac{e\alpha}{\hbar}\Psi^\dagger\sigma_x\Psi\mathbf{u}_y. \tag{14}$$

In the framework of second quantization, Ψ becomes a field operator, which may be expanded using a convenient basis such as the SO coupling stationary states.

B. Expansion of the field operator

The first step is to define the creation and annihilation operators for the SO coupling stationary states. We begin by introducing the creation operators in the original, noninteracting spin basis: $\hat{a}^\dagger_{\gamma ks}$ ($\hat{b}^\dagger_{\gamma ks}$) creates an incoming (outgoing) electron with spin $s\in\{\uparrow,\downarrow\}$ in lead γ with longitudinal momentum k in the state $|a,k,s\rangle_\gamma$ ($|b,k,s\rangle_\gamma$), where $|\epsilon,k,s\rangle_\gamma=e^{i\eta_\epsilon kx_\gamma}|s\rangle$. These standard operators satisfy the anticommutation relation $[\hat{a}_{\gamma,k,s},\hat{a}^\dagger_{\beta,k',s'}]_+=\delta_{kk'}\delta_{\gamma\beta}\delta_{ss'}$. Through Eq. (8), we now introduce $\hat{a}^\dagger_{\gamma k\sigma}$, which creates an incoming electron in lead γ with longitudinal momentum k and spin-orbit coupling label $\sigma\in\{+,-\}$ (not to be confused with the spin s) satisfying the relation

$$\hat{a}^\dagger_{\gamma k\sigma}=\frac{1}{\sqrt{2}}[e^{i\theta_\gamma/2}\hat{a}^\dagger_{\gamma k\uparrow}+\eta_\sigma e^{-i\theta_\gamma/2}\hat{a}^\dagger_{\gamma k\downarrow}]. \tag{15}$$

Knowing the anticommutation relationship in the spin basis, we can calculate it in the new, stationary, spin-orbit coupling basis to be

$$[\hat{a}_{k,\gamma,\sigma},\hat{a}^\dagger_{k',\beta,\sigma'}]_+=\delta_{kk'}\delta_{\alpha\beta}\delta_{\sigma\sigma'}, \tag{16}$$

where we used the relation $\eta_\sigma\eta_{\sigma'}=2\delta_{\sigma\sigma'}-1$. This result provides justification for our designation of the SO coupling eigenstates and the usage of the spin-orbit coupling label σ rather than the spin *s*. The stationary states form a complete basis, and we can use them to expand the field operator in lead γ. For notational convenience, we will choose from here on to align x_γ and y_γ with the reference axes $x_{\mathrm{ref}}\to x$ and $y_{\mathrm{ref}}\to y$ (so that $\theta_\gamma=\pi/2$) and specifically track the angular dependence of the leads in the scattering matrix. The field operator is

$$\hat{\Psi}(x,y)_\gamma=\sum_{\sigma,\epsilon}\sum_{k=-\eta_\sigma k_o}^{\infty}\hat{\epsilon}_{\gamma,k,\sigma}\chi^\epsilon_\sigma\frac{e^{i\eta_\epsilon kx}\Phi(y)}{\sqrt{L}}, \tag{17}$$

where $\hat{\epsilon}=\hat{a}$ ($\hat{b}$) is the annihilation operator in the incoming (outgoing) states and χ^ϵ_σ is a two-component spinor obtained from Eq. (8) by setting $\theta_\gamma=\pi/2$,

$$|\epsilon,k,\sigma\rangle_\gamma=\frac{e^{i\eta_\epsilon kx}\Phi(y)}{\sqrt{L}}\underbrace{\begin{bmatrix}\dfrac{1+i}{2}\\ \eta_\epsilon\eta_\sigma\dfrac{1-i}{2}\end{bmatrix}}_{\chi^\epsilon_\sigma}. \tag{18}$$

As shown in Fig. 4, the spin of χ^ϵ_σ depends on the SO coupling state σ and on the direction of propagation ϵ.

At this point, it is more convenient to go from a discrete sum in k space to a continuous integral in energy by defining the operators $\hat{a}^{\dagger}(E)$, which create electrons in the energy quasicontinuum. As our labeling defines a one-to-one correspondence between (ϵ,k,σ) and (ϵ,E,σ), we can define unambiguously $\hat{a}^{\dagger}_{\gamma\sigma}(E)=\sqrt{\rho(E)}\hat{a}^{\dagger}_{\gamma k\sigma}$, so that

$$[\hat{a}_{\gamma,\sigma}(E),\ \hat{a}^{\dagger}_{\beta,\sigma'}(E')]_{+}=\delta_{\gamma\beta}\delta_{\sigma\sigma'}\delta(E-E'), \tag{19}$$

where $\rho(E)$ is the density of states at energy E. It is shown in Appendix A that $\rho(E)$ is independent of the spin-orbit coupling label σ. Replacing the discrete sum over k by an integral over E and introducing the new operators and their time dependence $\hat{a}(E,t)=e^{-i(E/\hbar)t}\hat{a}(E)$, we find

$$\hat{\Psi}(x,y,t)_{\gamma}=\frac{1}{\sqrt{2\pi}}\sum_{\sigma,\epsilon}\int_{E_0}^{\infty}\frac{dE}{\sqrt{\hbar v_g(E)}}\hat{\epsilon}_{\gamma,\sigma}(E)\chi^{\epsilon}_{\sigma}\Phi(y)\times e^{i\eta_{\epsilon}k(E,\sigma)x}e^{-i(E/\hbar)t}, \tag{20}$$

with $E_0\equiv -m\alpha^2/2\hbar^2$, and k has been replaced by $k(E,\sigma)$ to remind us that k depends on the spin-orbit coupling label σ for a given energy E.

C. Current in the spin-orbit coupling basis

The current in lead γ is given by

$$\hat{I}_{\alpha}=\int dy\hat{j}_x=\int dy(\hat{j}_{x\mathrm{K}}+\hat{j}_{x\mathrm{SO}})\equiv\hat{I}_{\mathrm{K}}+\hat{I}_{\mathrm{SO}}. \tag{21}$$

We will begin by calculating the kinetic term $\hat{I}_{\mathrm{K}}$. Using Eq. (13), we have

$$\hat{I}_{\mathrm{K}}(t)=\sum_{\sigma\sigma'}\sum_{\epsilon\epsilon'}\int dEdE' I^{\epsilon\epsilon'}_{\mathrm{K}\sigma\sigma'}(E,E')\hat{\epsilon}^{+}_{\gamma\sigma}(E)\times\hat{\epsilon}'_{\gamma\sigma'}(E')e^{i[(E-E')/\hbar]t}, \tag{22}$$

$$I^{\epsilon\epsilon'}_{\mathrm{K}\sigma\sigma'}(E,E')=\frac{e\hbar}{2mi}\frac{i\chi^{\epsilon\dagger}_{\sigma}\chi^{\epsilon'}_{\sigma'}}{h\sqrt{v_g(E)v_g(E')}}[\eta_{\epsilon}k(E,\sigma)+\eta_{\epsilon'}k(E',\sigma')]e^{i[\eta_{\epsilon'}k(E',\sigma')-\eta_{\epsilon}k(E,\sigma)]x}. \tag{23}$$

We notice from Eq. (22) that the frequency ω of the current is given by $\hbar\omega=E-E'$. Following Ref. 15, we calculate the current and noise in the zero-frequency limit and make the approximation $k(E',\sigma)\approx k(E,\sigma)$ (as $E\approx E'$) for electrons having the same SO coupling label and, using Eq. (9), $k(E',\sigma')=k(E,\sigma)+\eta_{\sigma}\Delta k$ for electrons having different SO coupling labels. From Eq. (18), we also have (with $\delta_{\epsilon\neq\epsilon'}=1$ if $\epsilon\neq\epsilon'$, 0 otherwise)

$$\chi^{\epsilon\dagger}_{\sigma}\chi^{\epsilon'}_{\sigma'}=\delta_{\epsilon\epsilon'}\delta_{\sigma\sigma'}+\delta_{\epsilon\neq\epsilon'}\delta_{\sigma\neq\sigma'}. \tag{24}$$

This result is consistent with the fact that only electrons with the same direction of propagation and the same spin-orbit coupling label or opposite direction of propagation and opposite spin-orbit coupling label have the same spin.

In the $\sigma=\sigma'$ case, implying $\epsilon=\epsilon'$ and $k(E',\sigma')\approx k(E,\sigma)$, we find (see also Appendix A)

$$I^{\epsilon\epsilon'}_{\mathrm{K}\sigma\sigma'}(E,E')|_{\sigma=\sigma'}=\eta_{\epsilon}\frac{e}{h}\frac{k(E,\sigma)}{k(E,\sigma)+\eta_{\sigma}\dfrac{m\alpha}{\hbar^2}}. \tag{25}$$

In the $\sigma\neq\sigma'$ case, implying $\epsilon\neq\epsilon'$ and $k(E',\sigma')\approx k(E,\sigma)+\eta_{\sigma}2m\alpha/\hbar^2$, so that $\eta_{\epsilon}k(E,\sigma)+\eta_{\epsilon'}k'(E,\sigma')=-\eta_{\epsilon}\eta_{\sigma}2m\alpha/\hbar^2$, we find

$$I^{\epsilon\epsilon'}_{\mathrm{K}\sigma\sigma'}(E,E')|_{\sigma\neq\sigma'}=-\eta_{\epsilon}\frac{e}{h}\frac{\eta_{\sigma}\dfrac{m\alpha}{\hbar^2}}{k(E,\sigma)+\eta_{\sigma}\dfrac{m\alpha}{\hbar^2}}\times e^{-i\eta_{\epsilon}[2k(E,\sigma)+\eta_{\sigma}\Delta k]x}. \tag{26}$$

If we only consider the kinetic term of the current, a nonvanishing contribution for $\epsilon\neq\epsilon'$ leads to terms like $\hat{a}^{\dagger}\hat{b}$ and $\hat{b}^{\dagger}\hat{a}$ in the expression of the current, corresponding to electrons propagating in opposite directions.

We now consider the contribution of the spin-orbit coupling current $\hat{I}_{\mathrm{SO}}$. Using Eq. (14) to calculate $I^{\epsilon\epsilon'}_{\mathrm{SO}\sigma\sigma'}$ in Eq. (22) with $\mathrm{K}\rightarrow\mathrm{SO}$, we find

$$I^{\epsilon\epsilon'}_{\mathrm{SO}\sigma\sigma'}(E,E')=-\frac{e}{h}\frac{\dfrac{\alpha}{\hbar}}{\sqrt{v_g(E)v_g(E')}}\times\chi^{\epsilon\dagger}_{\sigma}\sigma_y\chi^{\epsilon'}_{\sigma'}e^{i[\eta_{\epsilon'}k(E',\sigma')-\eta_{\epsilon}k(E,\sigma)]x}. \tag{27}$$

Using $\eta_{\epsilon'}\eta_{\sigma'}=\eta_{\epsilon}\eta_{\sigma}$, we have from Eq. (18) that $\sigma_y\chi^{\epsilon'}_{\sigma'}=-\eta_{\epsilon'}\eta_{\sigma'}\chi^{\epsilon'}_{\sigma'}$ and $\chi^{\epsilon\dagger}_{\sigma}\sigma_y\chi^{\epsilon'}_{\sigma'}=-\eta_{\epsilon}\eta_{\sigma}(\delta_{\epsilon\epsilon'}\delta_{\sigma\sigma'}+\delta_{\epsilon\neq\epsilon'}\delta_{\sigma\neq\sigma'})$, so that

$$I^{\epsilon\epsilon'}_{\mathrm{SO}\sigma\sigma'}(E,E')=\eta_{\epsilon}\frac{e}{h}\frac{\eta_{\sigma}\dfrac{m\alpha}{\hbar^2}}{k(E,\sigma)+\eta_{\sigma}\dfrac{m\alpha}{\hbar^2}}[\delta_{\epsilon\epsilon'}\delta_{\sigma\sigma'}+e^{-i\eta_{\epsilon}[2k(E,\sigma)+\eta_{\sigma}\Delta k]x}\delta_{\epsilon\neq\epsilon'}\delta_{\sigma\neq\sigma'}]. \tag{28}$$

We can now calculate the value of the total current from Eqs. (25), (26), and (28),

$$I^{\epsilon\epsilon'}_{\sigma\sigma'}(E,E')=I^{\epsilon\epsilon'}_{\mathrm{K}\sigma\sigma'}(E,E')+I^{\epsilon\epsilon'}_{\mathrm{SO}\sigma\sigma'}(E,E')=\eta_{\epsilon}\frac{e}{h}\delta_{\epsilon\epsilon'}\delta_{\sigma\sigma'}. \tag{29}$$

Although the spin-orbit coupling mixes electron states having different directions of propagation when we consider only the kinetic term of the current, these contributions can-

cel when we add the spin-orbit coupling current I_{SO}, and we find the standard formula for the current operator,

$$\hat{I}_\alpha(t)=\frac{e}{h}\sum_\sigma \int dEdE'[\hat{a}^\dagger_{\alpha\sigma}(E)\hat{a}_{\alpha\sigma}(E') - \hat{b}^\dagger_{\alpha\sigma}(E)\hat{b}_{\alpha\sigma}(E')]e^{i[(E-E')/\hbar]t}. \quad (30)$$

The definition of the $\hat{a}$ ($\hat{b}$) operators as corresponding to states with positive (negative) group velocity, and not necessarily positive (negative) wave vector, is consistent with the fact that they carry the current in opposite directions. More importantly, the final expression of the current is similar to the one found in Ref. 15, but with the spin index replaced by the spin-orbit coupling label $\sigma=\pm$. The spin related to this new index depends on the direction of propagation, that is, the angle θ_γ of the lead. Therefore, we expect a θ dependence in the scattering matrix relating the outgoing states in the outputs ($\hat{b}$ states) to the incident states at the input ($\hat{a}$ states),

$$\hat{b}_{\gamma\rho}(E)=\sum_{\beta\sigma} S^{\gamma\rho}_{\beta\sigma}(E,\theta_\gamma,\theta_\beta)\hat{a}_{\beta\sigma}(E), \quad (31)$$

where both ρ and σ indicate the spin-orbit coupling label. The current operator can then be written

$$\hat{I}_\alpha(t)=\frac{e}{h}\sum_\rho\sum_{\sigma\sigma'}\sum_{\beta\gamma}\int dEdE' e^{i(E-E')t/\hbar} \times \hat{a}^\dagger_{\beta\sigma}(E)A^{\alpha\rho}_{\beta\gamma\sigma\sigma'}(E,E')\hat{a}_{\gamma\sigma'}(E'), \quad (32)$$

$$A^{\alpha\rho}_{\beta\gamma\sigma\sigma'}(E,E')=\delta_{\alpha\beta}\delta_{\alpha\gamma}\delta_{\rho\sigma}\delta_{\rho\sigma'} - S^{*\alpha\rho}_{\beta\sigma}(E,\theta_\alpha,\theta_\beta)S^{\alpha\rho}_{\gamma\sigma'}(E',\theta_\alpha,\theta_\gamma). \quad (33)$$

The unilateral power spectral density is defined as twice the Fourier transform of the symmetrized correlator of the current fluctuations,[41]

$$S_{\alpha\beta}(\omega)=\int d\tau e^{i\omega\tau}\langle \delta\hat{I}_\alpha(\tau)\delta\hat{I}_\beta(0)+\delta\hat{I}_\beta(0)\delta\hat{I}_\alpha(\tau)\rangle, \quad (34)$$

where $\delta\hat{I}_\alpha(t)\equiv\hat{I}_\alpha(t)-\langle\hat{I}_\alpha\rangle$, and we have assumed stationarity. In the following, we consider the noise power in the $\omega\to 0$ limit and energy-independent scattering matrices in a particular lead α,

$$S_{\alpha\alpha}(0)=\frac{2e^2}{h}\sum_{\rho\rho'}\sum_{\gamma\delta}\sum_{\sigma\sigma'}A^{\alpha\rho}_{\gamma\delta\sigma\sigma'}A^{\alpha\rho'}_{\delta\gamma\sigma'\sigma} \times\int dE f_{\gamma\sigma}(E)[1-f_{\delta\sigma'}(E)], \quad (35)$$

where $f_{\gamma\sigma}(E)$ is the Fermi-Dirac distribution in lead γ for electrons with SO label σ.

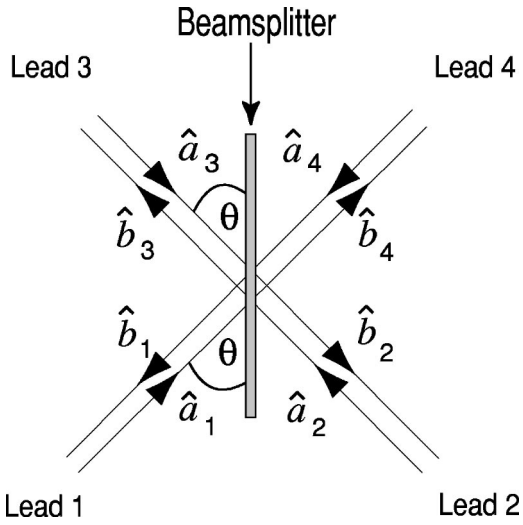

FIG. 5. Four-port electron beam splitter. The operators $\hat{a}_i$ ($\hat{b}_i$) annihilate electrons entering (leaving) the device through port *i*. It is assumed that Fermi-degenerate, single-mode electron sources inject electrons towards the beam splitter. The beam splitter is a sharp potential barrier.

IV. SPIN-ORBIT COUPLING AND NOISE IN ELECTRON COLLISIONS

We will now use the expression of the current operator, unilateral power spectral density, and the scattering matrix to calculate the current, noise power, and Fano factor in several experiments using the four-port beam splitter setup. The experiments include an unpolarized electron collision, which has already been experimentally demonstrated (see Ref. 6), and a spin-polarized electron collision. We will show that a noise measurement upon collision of polarized electrons at an electron beam splitter provides an experimental means to measure the Rashba parameter α. We also consider a collision between EPR-type entangled electrons. We show that the degree of maximal bunching for the spin-singlet state depends on the lead orientation of the beam splitter.

A. Electron beam splitter

The electron beam splitter is a four-port device (two input and two output leads), such as the one shown in Fig. 5. It is a ''spatial beam splitter''; it only operates on the spatial or orbital subspace of the electrons (counterexample, a polarization beam splitter). In the spin-independent transport case, the scattering matrix does not mix different spins, because the beam splitter only acts on the electron orbital states and there is no spin-orbit coupling. In this case, the reflection and transmission coefficients are independent of the spin. However, the situation is more complicated when we include spin-orbit coupling, because the spin associated with the spin-orbit coupling label σ is different in each lead (the leads having different orientations). The beam splitter still only operates on the electron orbital states, but there is now a connection from orbit to spin through the spin-orbit coupling. The conservation of the spin at the beam splitter implies that we have a mixing of the spin-orbit states (off-

diagonal elements in the scattering matrix), and this mixing becomes more important when the angle between the leads increases.

A beam splitter, with all leads oriented at the same angle θ with respect to the beam splitter (the case illustrated in Fig. 5), is investigated in Appendix B, and the following scattering matrix is found after some simplifying assumptions:

$$\begin{pmatrix} \hat{b}_{3,+} \\ \hat{b}_{3,-} \\ \hat{b}_{4,+} \\ \hat{b}_{4,-} \end{pmatrix} = \underbrace{\begin{pmatrix} r\cos\theta & ir\sin\theta & t & 0 \\ ir\sin\theta & r\cos\theta & 0 & t \\ t & 0 & r\cos\theta & -ir\sin\theta \\ 0 & t & -ir\sin\theta & r\cos\theta \end{pmatrix}}_{S} \times \begin{pmatrix} \hat{a}_{1,+} \\ \hat{a}_{1,-} \\ \hat{a}_{2,+} \\ \hat{a}_{2,-} \end{pmatrix}. \tag{36}$$

We note that the unitarity of the S matrix requires $|r|^2 + |t|^2 \equiv R + T = 1$ and $rt^* + tr^* = 0$.

As an example of an experimental realization of an electron beam splitter, we consider the devices used in Refs. 5 and 6. In those experiments, each port of the electron beam splitter comprises a quantum point contact[2,3] (QPC) defined electrostatically by negative voltages applied to Schottky gates.[6] At cryogenic temperatures, the input QPC's at leads 1 and 2 serve as Fermi-degenerate, single-mode electron sources and are typically biased at[6,11] or below[5,11] the first conductance plateau. The output QPC's at leads 3 and 4 are typically biased ''wide open'' to collect all electrons from the beam splitter device without reflecting any back towards the beam splitter. The beam splitter itself is also defined electrostatically by a narrow Schottky gate in close proximity to the 2DEG to provide a sharp potential barrier.[6] A small voltage is applied to tune the beam splitter transmission probability T.

At cryogenic temperatures, the transport through the beam splitter device is ballistic; the electrons are coherent across the entire device.[6,5,11] The total area of the beam splitter device is smaller than 1 μm $\times 1$ μm, while the inelastic phonon scattering and elastic ionized impurity scattering lengths are typically larger than this characteristic size. This leaves only the elastic scattering at the beam splitter itself. Furthermore, the screening length (typically 5 nm) is assumed to be much smaller than the Fermi wavelength (typically 40 nm), so Coulomb interaction can be neglected. Consequently, the interactions related to quantum interference will occur in this device, while those related to the Coulomb charge of the electrons can be ignored.

In Refs. 5 and 6, the beam splitter is operated by applying a drain-source voltage V_{ds} to leads 1 and/or 2 with respect to leads 3 and 4. A modulation of V_{ds} is used with synchronous detection to allow the measurement of the low-frequency ($\hbar\omega \ll eV_{ds}$) nonequilibrium transport noise due to electrons in the net-transport energy window $[E_f, E_f + eV_{ds}]$. At temperature $\Theta = 0$, the input QPC's act as single-mode, Fermi-degenerate sources. For the single transverse mode accomodated by the QPC's, the associated longitudinal modes in the net-transport energy window $[E_f, E_f + eV_{ds}]$ are fully occupied. On the output side, the modes in the same net-transport energy window are unoccupied. Of course, all modes below the Fermi energy E_f are also fully occupied. For the finite-temperature case, this physical picture remains valid for $eV_{ds} \gg k_B\Theta$. We note here that the precise means for achieving a Fermi-degenerate source depends on the type of experiment (polarized collision, for example). For our purposes here, we will assume that an appropriate Fermi-degenerate source exists and injects electrons towards the beam splitter for each experiment described below.

Finally, the beam splitter is considered ''linear,'' in the sense that it operates on single-electron modes and does not mix energies. In isolation, each electron mode that impinges on the beam splitter will have a probability T to be transmitted and R to be reflected. However, quantum mechanical interference effects between identical electrons[6] or entangled electron states[9–11] that impinge upon the beam splitter may alter the single-particle transmission and reflection properties in scattering experiments.

B. Manifestations of spin-orbit coupling

The coherent scattering formalism derived here can be used generally for several different experimental realizations of spin-orbit coupling, for example, in the following cases (note that global spin-orbit coupling means that the entire device is described by the SO Hamiltonian, whereas local spin-orbit coupling implies the SO Hamiltonian applies only locally).

(i) Global spin-orbit coupling, $\sigma = \pm$ equilibrium leads, unpolarized and polarized $\sigma = \pm$ state transport.

(ii) Global spin-orbit coupling, $\sigma = \pm$ equilibrium leads, polarized and unpolarized $s = \uparrow\downarrow$ state transport injected at energies above the equilibrium leads.

(iii) Global spin-orbit coupling, $\sigma = \pm$ equilibrium leads, entangled $\sigma = \pm$ state transport.

(iv) Global spin-orbit coupling, $\sigma = \pm$ equilibrium leads, entangled $s = \uparrow\downarrow$ state transport.

(v) Local spin-orbit coupling, $s_{\uparrow\downarrow}$ equilibrium leads that adiabatically and coherently enter and leave the local spin-orbit coupling region, unpolarized, polarized, and entangled $s = \uparrow\downarrow$ state transport.

Although this list is not exhaustive, it does represent the variety of systems that can be analyzed using the SO coupling coherent scattering formalism. The experimental results depend on the manner in which spin-orbit coupling manifests itself in the system and, of course, the particular experiment implemented. As examples, we consider below the current and collision noise at an electron beam splitter for a few of the specific cases listed above.

C. Electron partition noise: Case 1

This experiment uses an electron beam splitter in a system with global spin-orbit coupling. The equilibrium stationary states are the $\sigma = \pm$ states, and, consequently, the equilibrium leads at zero temperature are Fermi degenerate upto the

Fermi energy. A small bias voltage V_{ds} is applied to lead 1 with respect to leads 2, 3, and 4. Both $\sigma=+$ and $\sigma=-$ states impinge on the beam splitter from port 1 and are subsequently partitioned into ports 3 and 4 according to the scattering matrix in Eq. (36). Using Eqs. (32) and (35), we find the current, unilateral power spectral density, and Fano factor in port 4 to be

$$\langle \hat{I}_4 \rangle = \frac{2e^2}{h} T V_{ds}, \tag{37}$$

$$S_{44}(0) = \frac{2e^2}{h} 2T(1-T) e V_{ds}, \tag{38}$$

$$F \equiv \frac{S_{44}(0)}{2e\langle \hat{I}_4 \rangle} = 1 - T. \tag{39}$$

We have omitted the minus sign for the current which indicates that the current is leaving the device. We find standard partition noise for this case, identical to the results expected for a Fermi degenerate $s=\uparrow\downarrow$ system in the absence of spin-orbit coupling. Analogously, injecting polarized electrons in the σ basis will halve the current and power spectral density, but leave the Fano factor unchanged. We note that the similarity between the s and σ bases exists, in part, because we are effectively looking at the charge when measuring the current and power spectral density. When we figuratively count the charges that reflect to lead 3, we get the same number in both cases. We can conclude that a partition noise experiment using a spatial beam splitter under the conditions of case 1 will not reveal experimentally the spin-orbit coupling effect.

D. Spin-unpolarized electron collision: Case 1

We now consider the same system with leads 1 and 2 biased with respect to leads 3 and 4. Again, there is global spin-orbit coupling, and the equilibrium $\sigma=\pm$ stationary states are Fermi degenerate up to the Fermi energy. In addition, the modes in leads 1 and 2 within the net-transport energy window $[E_F, E_F+eV_{ds}]$ are also Fermi degenerate, while the modes in the same net-transport energy window in leads 3 and 4 on the output side are unoccupied. Electrons in leads 1 and 2 within the net-transport energy window collide at the beam splitter and, subsequently, exit through the unoccupied states in leads 3 and 4.

In the case without SO coupling, each electron mode in lead 1 has an identical partner in lead 2. During the collision process, these electron modes impinge upon the beam splitter and quantum mechanically interfere. This quantum interference, i.e., the Pauli exclusion principle, forbids the two identical electrons to exit through the same output lead. Therefore, the two identical electrons from leads 1 and 2 must leave the device in an antibunched manner: one electron through lead 3 and one electron through lead 4. This is true for each mode in the net-transport energy window. Since the input leads are Fermi degenerate and noiseless in the zero-frequency limit, the outputs are also noiseless. We expect a total suppression of the partition noise.[6,15]

With spin-orbit coupling, we do not expect this result to be modified, because the leads remain Fermi degenerate for both spins $\sigma=\pm$ in the zero-temperature limit. To gain intuition, we note that a linear beam splitter does not couple modes at different energies, and so the aggregate collision can be viewed as a two-particle collision for each mode that makes up the net-transport energy window. Therefore, we consider the collision of four electrons at the same energy. The initial state is

$$|\Psi_i\rangle = \hat{a}^\dagger_{1+}(E)\hat{a}^\dagger_{1-}(E)\hat{a}^\dagger_{2+}(E)\hat{a}^\dagger_{2-}(E)|0\rangle. \tag{40}$$

The output state is found using Eqs. (31) and (36),

$$\begin{aligned}|\Psi_f\rangle &= [r[\cos\theta\hat{b}^\dagger_{3+} + i\sin\theta\hat{b}^\dagger_{3-}] + t\hat{b}^\dagger_{4+}] \\ &\times [r[i\sin\theta\hat{b}^\dagger_{3+} + \cos\theta\hat{b}^\dagger_{3-}] + t\hat{b}^\dagger_{4-}] \\ &\times [t\hat{b}^\dagger_{3+} + r[\cos\theta\hat{b}^\dagger_{4+} - i\sin\theta\hat{b}^\dagger_{4-}]] \\ &\times [t\hat{b}^\dagger_{3-} + r[-i\sin\theta\hat{b}^\dagger_{4+} + \cos\theta\hat{b}^\dagger_{4-}]]|0\rangle \\ &= \hat{b}^\dagger_{3+}\hat{b}^\dagger_{3-}\hat{b}^\dagger_{4+}\hat{b}^\dagger_{4-}|0\rangle,\end{aligned} \tag{41}$$

where we have used the relation $r^4+t^4-2r^2t^2=1$. As expected, a full occupation of the input states at energy E leads to a full occupation of the output states.

For degenerate inputs at leads 1 and 2, we find the general result for the current, unilateral spectral density, and Fano factor in lead 4 using Eqs. (32), (35), and (36):

$$\langle \hat{I}_4 \rangle = \frac{2e^2}{h} V_{ds}, \tag{42}$$

$$S_{44}(0) = 0, \tag{43}$$

$$F \equiv \frac{S_{44}(0)}{2e\langle \hat{I}_4 \rangle} = 0. \tag{44}$$

Because the input leads are Fermi degenerate, a calculation of the current noise in the output leads shows a complete suppression of the partition noise. Even though the beam splitter in the presence of SO coupling will couple spin states, from the final-state point of view, the Pauli exclusion principle requires a Fermi-degenerate occupation of the $\sigma=\pm$ states in leads 3 and 4 given a Fermi-degenerate input at leads 1 and 2. The only difference with the spin-independent transport case is that the colliding electrons at the same energy do not have the same momentum ($k \neq k'$). Therefore, we can conclude that a collision experiment of unpolarized $\sigma=\pm$ electrons cannot reveal SO coupling in the system. Consequently, the nonideality in the noise suppression observed in Ref. 6 cannot be attributed to SO coupling.

E. Spin-polarized electron collision: Case 1

In the previous example, an unpolarized collision cannot show any SO coupling effect, because, starting with two Fermi-degenerate sources, the collision statistics are governed by the Pauli exclusion principle independent of the SO coupling. The same argument holds true for a spin-polarized

collision in the absence of SO coupling. However, this is not the case for a spin-polarized collision in the presence of SO coupling.

We consider the same collision experiment as above, but we assume a means to inject electrons polarized with spin σ within the net-transport window from leads 1 and 2. These polarized electron collide at the beam splitter and exit through ports 3 and 4. For example, we consider electrons polarized in the $\sigma=+$ state. The $\sigma=+$ states are completely occupied within the net-transport window, but the $\sigma=-$ states are completely empty above the Fermi energy. Using Eqs. (32), (35), and (36), we find

$$\langle \hat{I}_4 \rangle = \frac{e^2}{h} V_{ds}, \tag{45}$$

$$S_{44}(0) = \frac{2e^2}{h} 2T(1-T)\sin^2\theta e V_{ds}, \tag{46}$$

$$F \equiv \frac{S_{44}(0)}{2e\langle \hat{I}_4 \rangle} = 2T(1-T)\sin^2\theta. \tag{47}$$

There is now residual partition noise at the outputs. The physics can be understood in the following way. Upon collision, quantum interference (the Pauli exclusion principle) forbids identical electrons from leaving through the same port. However, the beam splitter mixes the $\sigma=+$ states with the $\sigma=-$ states upon reflection, while leaving the $\sigma=+$ states unaltered upon transmission. Therefore, the quantum interference is imperfect. From the scattering matrix in Eq. (36), we find that the probability of a $\sigma=+$ state to be reflected to a $\sigma=-$ state is $(1-T)\sin^2\theta$. The probability that a $\sigma=+$ state is transmitted to a $\sigma=+$ state is T. Therefore, identical $\sigma=+$ electrons from leads 1 and 2 can both leave through port 4 as a transmitted $\sigma=+$ and a reflected $\sigma=-$ electron with probability $T(1-T)\sin^2\theta$. The same holds for both electrons leaving through port 3. The incomplete suppression of the partition noise is due to incomplete quantum interference, and this is directly related to the incomplete ''overlap'' (the degree to which they are no longer identical) of the electrons at the output ports. If we consider a $T=1/2$ beam splitter, we find a Fano factor

$$F(T=1/2) = \tfrac{1}{2}\sin^2\theta, \tag{48}$$

which corresponds to standard partition noise for the fraction $\sin^2\theta$ of the electrons which do not remain identical upon collision.

F. Spin-polarized electron collision: Case 2

We now consider a different version of the spin-polarized collision experiment. In case 2, the leads remain Fermi degenerate in the σ basis, but the injected spins are polarized in the spin s basis. For example, we consider $s=\uparrow$ electrons being injected into the beam splitter device from leads 1 and 2. For our purposes here, we assume these electrons are injected in a degenerate manner; that is, the injected modes are completely occupied. As shown in Fig. 6, the injected electrons fall in a range of momenta $[k_1,k_2]$ with corresponding

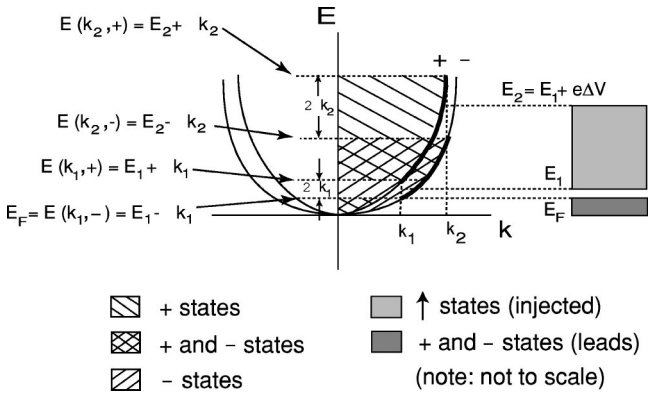

FIG. 6. Energy diagram for polarized-spin injection, case 2, $e\Delta V \geqslant \alpha k_1 + \alpha k_2$. Spin $s=\uparrow$ electrons are injected into an electron beam splitter device with equilibrium leads in the SO coupling basis. The $s=\uparrow$ electrons are assumed to fall within the energy window $[E_1, E_2 \equiv E_1 + e\Delta V]$, such that the lowest-energy injected $s=\uparrow$ electron at energy $E=E_1$ has a $\sigma=-$ component at the lead Fermi energy $E_F = E_1 - \alpha k_1$. In terms of the SO coupling stationary states, the jointly occupied $\sigma_\pm$ states occur in the crosshatched energy range; these states will not contribute to the collision noise. The fraction $\alpha(k_1+k_2)/e\Delta V \leqslant 1$ of the total states are only unilaterally occupied (diagonal lines only); these states partially contribute to the partition noise through the factor $\sin^2\theta$ depending on the lead orientation.

energies E_1 and $E_2 = E_1 + e\Delta V$ in the absence of SO coupling. Here, $e\Delta V \geqslant \alpha k_1 + \alpha k_2$ is defined as the energy width of the net-transport window in analogy to an applied voltage. Once injected into the device with SO coupling, the spin-up electrons with momenta $[k_1,k_2]$ project onto the $\sigma=\pm$ states with energies $[E_1 \pm \alpha k_1, E_2 \pm \alpha k_2]$. Note that we have chosen the energy E_1 to be the minimum energy an $s=\uparrow$ electron can have such that its $\sigma=-$ component remains above the $\sigma_\pm$ Fermi level, i.e., $E_F = E_1 - \alpha k_1$.

As the s spin basis is not the stationary basis and because the SO coupling scattering matrix mixes different SO coupling states, we again expect some of the partition noise to be recovered in a polarized-spin collision. The degree of partition noise recovery in this case depends on the SO coupling constant α and on the angle between the colliding leads. We will confirm this by calculating the nonequilibrium noise of the electrons in the net-transport energy window $[E_1,\ E_1 + e\Delta V]$, assuming that the process of polarization does not effect the transport in the conductor (for example, if a magnetic field is used to polarize the electrons, this field does not leak into the beam splitter device region). Using Eqs. (32), (35), and (36) and the energy band diagram shown in Fig. 6, we find

$$\langle \hat{I}_4 \rangle = \frac{e^2}{h} \Delta V, \tag{49}$$

$$S_{44}(0) = \frac{2e^2}{h} 2T(1-T)\sin^2\theta(\alpha k_1 + \alpha k_2), \tag{50}$$

$$F = 2T(1-T)\sin^2\theta\left[\frac{\alpha k_1 + \alpha k_2}{e\Delta V}\right]. \tag{51}$$

The Fano factor is identical to the case 1 polarized collision [see Eq. (47)] for which only a fraction

$$\frac{1}{2}\frac{2\alpha k_1 + 2\alpha k_2}{e\Delta V} = \frac{\alpha k_1 + \alpha k_2}{e\Delta V} \leqslant 1$$

of the states undergo a polarized collision, and as in case 1, the partition noise is recovered through the factor $\sin^2\theta$. Note that a factor 1/2 comes out from the projection of the spin-up electrons onto the σ basis; the number of spin-up electrons in the energy window $[E_1, E_2]$ is the same as the number of $\sigma = +$ and $\sigma = -$ electrons in the energy window $[E_1 - \alpha k_1, E_2 + \alpha k_2]$.

This result can be explained using Fig. 6. In the input leads, the spin-up electron states between E_1 and E_2 are fully occupied. However, in terms of the SO coupling states, only the states between $E(k_1, +)$ and $E(k_2, -)$ are jointly occupied; just as in the unpolarized case [see Eq. (44)], these degenerate, identical states give no contribution to the noise upon collision due to the Pauli exclusion principle, i.e., quantum interference.

The fraction $(\alpha k_1 + \alpha k_2)/e\Delta V \leqslant 1$ of the injected states, however, is only unilaterally occupied; only the $-$ states are filled between $E(k_1, -)$ and $E(k_1, +)$, and only the $+$ states are filled between $E(k_2, -)$ and $E(k_2, +)$. These $+$ $(-)$ states at the input will reflect to identical $+$ $(-)$ states at the output with a reflection amplitude modified by $\cos\theta$ due to the lead orientation, while the transmission amplitude remains unmodified. In terms of probability, only the fractions $\cos^2\theta$ of these unilaterally occupied states from leads 1 and 2 remain identical in the output leads after collision. Therefore, the noise suppression due to the Pauli exclusion principle, quantum interference, occurs only for the faction $\cos^2\theta$ of the identical, unilaterally occupied electrons. Conversely, as was noted in the case 1 polarized collision, the $+$ $(-)$ states will reflect to the opposite $-$ $(+)$ states with a reflection amplitude modified by $\sin\theta$ due to the lead orientation, while the transmission amplitude preserves the $+$ $(-)$ states. Because these unilaterally occupied electron states are no longer identical after collision, the Pauli exclusion principle does not apply; there is no quantum interference. Therefore, the classical partition noise is partially recovered to the extent that the unilaterally occupied states are not identical, i.e., through the factor $\sin^2\theta = 1 - \cos^2\theta$.

In this treatment, we have assumed that the SO coupling is small $[(\alpha k_1 + \alpha k_2)/e\Delta V \leqslant 1]$, so that $E(k_1, +) \leqslant E(k_2, -)$. However, a typical value of the applied bias voltage is $eV = 0.1$–1.0 meV, which may be smaller than the typical values of the energy splitting caused by the Rashba effect ($0.3\ \text{meV} \leqslant 2\alpha k_1 \leqslant 3$ meV). In the $e\Delta V < \alpha k_1 + \alpha k_2$ case, none of the net-transport electrons interfere at the beam splitter and so all of the electrons contribute to the partition noise, $F = 2T(1-T)\sin^2\theta$. The $e\Delta V < \alpha k_1 + \alpha k_2$ results are identical to the case 1 polarized collision results in Eqs. (45)–(47) with eV_{ds} replaced by $e\Delta V$.

This experiment provides a new means to determine the Rashba splitting parameter. Depending on the bias voltage ΔV and the angle between the leads, the device can span the range from full noise suppression to the classical limit of the partition noise. Tuning the applied bias voltage and measuring the modification to the noise for a fixed lead orientation in this type of polarized collision provides a new experimental method to measure the Rashba parameter α.

G. Entangled-electron collision: Case 3

Finally, we consider the effect of global SO coupling on the collision of entangled-electron states. The collision of the spin-singlet ($\uparrow\downarrow$ spin-triplet) state from leads 1 and 2 at a spatial beam splitter yields bunched (antibunched) electrons at the output states 3 and 4 (Refs. 9 and 11) due to the orbital symmetry of the entangled-state wave function. We consider the modifications to this proposed experimental result due to global spin-orbit coupling.

We consider the simple case of two energy-degenerate, entangled electrons in the σ basis,

$$|\Psi_i\rangle = \frac{1}{\sqrt{2}}[\hat{a}^\dagger_{1+}(E)\hat{a}^\dagger_{2-}(E) - e^{i\phi}\hat{a}^\dagger_{1-}(E)\hat{a}^\dagger_{2+}(E)]|0\rangle. \tag{52}$$

The phase shift ϕ allows tuning of the entangled state from singlet to triplet through the factor $\cos^2(\phi/2)$.[11] An experimental proposal to realize this phase shift using a local spin-orbit coupling effect is discussed in Ref. 42. This state impinges on the beam splitter and quantum mechanically interferes with itself. At an output lead (for example, lead 4), one measures the noise power as a function of ϕ. Using Eqs. (32), (35), and (36), we find,

$$\langle \hat{I}_4 \rangle = \frac{e}{\rho(E)h}, \tag{53}$$

$$S_{44}(0) = \frac{2e^2}{\rho(E)h} 2T(1-T)\cos^2\theta\cos^2\frac{\phi}{2}, \tag{54}$$

$$F = 4T(1-T)\cos^2\theta\cos^2\frac{\phi}{2}, \tag{55}$$

where ρ is the density of states. For a $T = 1/2$ beam splitter, this result indicates that the Fano factor will oscillate with the phase ϕ between optimal antibunching ($F = 0$) and suboptimal bunching ($F = \cos^2\theta$) according to the orientation of the beam splitter leads. For a typical geometry with $\theta = \pi/4$, the oscillation will run between ideal antibunching ($F = 0$) and standard partition noise ($F = 1/2$). This simple example illustrates that the effects of global SO coupling should be included when considering entangled-electron experiments. Interestingly, a similar Fano factor dependence was found in Ref. 42 through an additional phase shift due to local, interband SO coupling.[40]

V. CONCLUSION

We have studied the influence of Rashba SO coupling in the framework of the Landauer-Büttiker formalism. Its main features are a spin splitting proportional to k and stationary states of the spin perpendicular to the direction of propagation. We included the effects of the Rashba SO coupling in the Landauer-Büttiker coherent scattering formalism. The Rashba SO coupling gave rise to two important modifications. First, the addition of a SO coupling term to the Hamiltonian modifies the expression of the current operator, resulting in an additional term directly related to the SO coupling. Second, the expansion of the current operator is performed in the basis of the Rashba SO coupling stationary states. The current operator was found to be identical to the one derived in the spin-independent transport case, but with the spin replaced by the SO coupling label. The main differences introduced by the SO coupling then arise in the calculation of the scattering matrix relating the Rashba SO coupling stationary states in different leads with different orientations. The direction of the spin depends on the direction of propagation, and this may be different for each lead in general. Therefore, the scattering matrix is shown to mix states with different SO coupling labels, and the strength of this mixing depends on the angle between the leads. The effect of SO coupling on the current noise was then investigated in several examples of electron collision. In the unpolarized-electron collision example, it is shown that the SO coupling does not modify the noise; this case is entirely determined by the Fermi degeneracy and the Pauli exclusion principle. In contrast, the polarized-spin s case exhibits a contribution to the noise caused by SO coupling, which is proportional to the SO coupling constant α and depends on the angle between the leads. A polarized electron collision experiment provides another means to measure the strength of the Rashba parameter α. In the case of a bunching-antibunching experiment with entangled electrons, the SO coupling also modifies the maximal degree of bunching one can achieve. Finally, this new formulation of the current operator can be applied to other coherent scattering experiments in which one wants to investigate or incorporate the effects of SO coupling.

ACKNOWLEDGMENTS

The authors gratefully acknowledge useful discussions with C. P. Master, E. Waks, and X. Maitre and the support of J. F. Roch. We thank the Quantum Entanglement Project (ICORP, JST) for financial support. W.D.O. gratefully acknowledges additional support from MURI and NDSEG.

APPENDIX A: DENSITY OF STATES WITH SPIN-ORBIT COUPLING

In this appendix, we calculate the density of states and show that it does not depend on the SO coupling label σ, as suggested by the symmetry between the + and − states in the energy dispersion diagram (see Fig. 2),

$$E=\frac{\hbar^2k^2(E,\sigma)}{2m}+\eta_\sigma\alpha k(E,\sigma), \tag{A1}$$

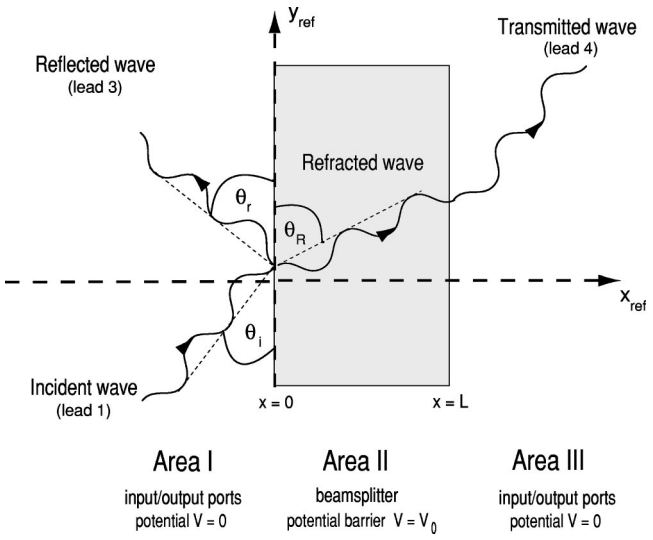

FIG. 7. Reflected, refracted, and transmitted waves in a beam splitter.

$$v_{g\sigma}(E)=\frac{1}{\hbar}\frac{dE(k,\sigma)}{dk}=\frac{\hbar k(E,\sigma)}{m}+\eta_\sigma\frac{\alpha}{\hbar}. \tag{A2}$$

From Eq. (9) we deduce

$$k(E,\sigma)=k(E,+)+(1-\eta_\sigma)\frac{m\alpha}{\hbar^2}, \tag{A3}$$

$$v_{g\sigma}(E)=\frac{\hbar k(E,\pm)}{m}\pm\frac{\alpha}{\hbar}\equiv v_g(E), \tag{A4}$$

$$\rho(E)=\frac{\rho(k)}{\hbar v_g(E)}=\frac{L}{2\pi}\frac{1}{\hbar v_g(E)}, \tag{A5}$$

which is independent of σ.

APPENDIX B: SCATTERING MATRIX IN THE FOUR-PORT BEAM SPLITTER CASE

Here, we determine the scattering matrix for the four-port beam splitter described in Fig. 5. The beam splitter is very simply approximated by a potential barrier at $V=V_0$ of length L. The plane is then divided into three areas of different potential (see Fig. 7) in which the solution of the Schrödinger equation is known.

Starting with an incident wave in lead 1, for example, we can calculate the reflected, refracted, and transmitted waves in leads 3 and 4, using the continuity of the wave function and its derivatives at the beam splitter interface ($x=0$ and $x=L$). For example, let us start with an incident state at energy E with momentum k_i in the SO coupling state $\sigma=+$. By the conservation of energy, the reflected wave in lead 3 is a superposition of the states $|\mathbf{k}_r(E,+),+\rangle$ and $|\mathbf{k}_r(E,-),-\rangle$ with

$$k_r(E,+)=k_i(E,+)=k_r(E,-)-\Delta k. \tag{B1}$$

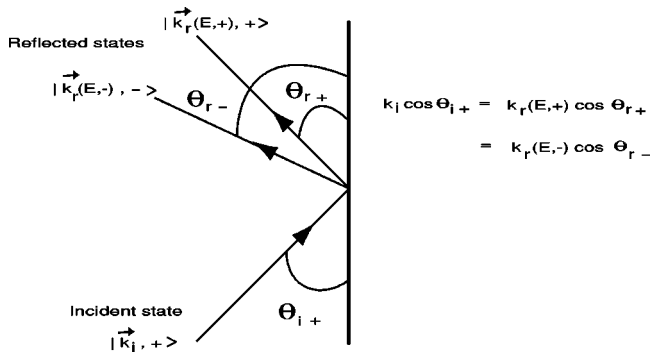

FIG. 8. Angular separation after reflection at a beam splitter.

The translational invariance of the beam splitter along the y axis leads to the conservation of the y component of the momentum:

$$k_i \cos\theta_i = k_r(E,+)\cos\theta_+ = k_r(E,-)\cos\theta_- . \quad \text{(B2)}$$

We deduce that $\cos\theta_i = \cos\theta_{r+}$, but $\cos\theta_i \neq \cos\theta_{r-}$. There is dispersion due to the SO coupling, leading to an angular separation between the $+$ and $-$ states after reflection at the beam splitter (see Fig. 8).

This angular separation is given by

$$\theta_{r-} = \arccos\left[\left(1 - \frac{\Delta k}{k_r(E,-)}\right)\cos\theta_i\right] \neq \theta_{r+} . \quad \text{(B3)}$$

Starting with an incident state with SO coupling label $-$, the angular separation is

$$\theta_{r+} = \arccos\left[\left(1 + \frac{\Delta k}{k_r(E,+)}\right)\cos\theta_i\right] \neq \theta_{r-} . \quad \text{(B4)}$$

In analogy with the total reflection for incident angles below the critical angle in classical optics, we can even have $[1+\Delta k/k_r(E,+)]\cos\theta_i > 1$, leading to a suppression of the reflection in the $+$ state for a small enough incident angle. We note that starting with a mixture of $+$ and $-$ states in the incident beam of electrons, one could suppress the reflection of the $+$ state, thus achieving a polarization of the beam. To be effective, one would require a strong SO coupling such as a locally enhanced Rashba effect in the beam splitter region.[42]

Here, we will neglect this effect of angular dispersion by considering only non-equilibrium electrons above the Fermi energy for which $\Delta k/k \ll 1$ (as the SO coupling is small compared to the kinetic energy) and the experimentally important incident angles ($\theta_i = \pi/4$). In this case, the angular separation is very small ($\Delta\theta = \theta_{r-} - \theta_{r+} \ll 1$). The equations of continuity of the wave function and its derivative are then much easier to solve, and one can find that the incident, refracted, and reflected waves have the same spin at $x=0$ and the refracted and transmitted waves have the same spin at $x=L$. Using Eq. (7) to find the spin overlap between different leads we find, starting with a $+$ incident state,

$$|\Psi_t\rangle = t|k,+\rangle, \quad |\Psi_r\rangle = r[\cos\theta_i|k,+\rangle + i\sin\theta_i|k,-\rangle], \quad \text{(B5)}$$

where $|\Psi_t\rangle$ is the transmitted wave (into lead 4) and $|\Psi_r\rangle$ the reflected wave (into lead 3). As the transmitted wave has the same direction of propagation as the incident wave, there is no mixing of the SO coupling states, and we have only the usual transmission coefficient t. For the reflected wave, the direction is changed and we have to mix the different SO coupling states to obtain the same spin as the incident wave on the interface with the beam splitter. If we start now with a $-$ incident state, we find

$$|\Psi_t\rangle = t|k,-\rangle, \quad |\Psi_r\rangle = r[i\sin\theta_i|k,+\rangle + \cos\theta_i|k,-\rangle]. \quad \text{(B6)}$$

The same analysis can be done for an incident state in lead 2 with θ_i replaced by $-\theta_i$. We then deduce the whole scattering matrix

$$S = \begin{bmatrix} r\cos\theta_i & ir\sin\theta_i & t & 0 \\ ir\sin\theta_i & r\cos\theta_i & 0 & t \\ t & 0 & r\cos\theta_i & -ir\sin\theta_i \\ 0 & t & -ir\sin\theta_i & r\cos\theta_i \end{bmatrix}. \quad \text{(B7)}$$

APPENDIX C: ALTERNATIVE DERIVATION OF POLARIZED COLLISION: CASE 2

In the main body of the text, we considered the direct application of Eq. (35) in the SO coupling basis to the calculation of the Fano factor. Although the direct application is more convenient, for completeness, we present here an alternative calculation of the Fano factor for a polarized collision, case 2 [Eq. (51)] with all operators expressed in the spin s basis.

The input state comprises electrons with the same spin, for example spin up, between k_1 and $k_2 = k(E_1 + e\Delta V)$ as shown in Fig. 6. We consider the initial state for the net-transport electrons and the current operator using the following notation:

$$|\Psi_i\rangle = \prod_{k=k_1}^{k_2} \hat{a}^\dagger_{1\uparrow}(k)\hat{a}^\dagger_{2\uparrow}(k)|0\rangle, \quad \text{(C1)}$$

$$\hat{I}_\alpha(t) = \frac{e}{h}\sum_\rho \sum_{\sigma\sigma'} \sum_{\beta\gamma} \int dE dE' e^{i(E-E')t/\hbar} A^{\alpha\rho}_{\beta\gamma\sigma\sigma'} \times \hat{a}^\dagger_{\beta\sigma}(E)\hat{a}_{\gamma\sigma'}(E'), \quad \text{(C2)}$$

$$A^{\alpha\rho}_{\beta\gamma\sigma\sigma'} = \delta_{\alpha\beta}\delta_{\alpha\gamma}\delta_{\rho\sigma}\delta_{\rho\sigma'} - S^{*\alpha\rho}_{\beta\sigma}S^{\alpha\rho}_{\gamma\sigma'}, \quad \text{(C3)}$$

where k_2 is given by $E_1 + e\Delta V = \hbar^2 k_2^2/2m$. We then use the current fluctuation $\delta\hat{I}_\alpha(t) = \hat{I}_\alpha(t) - \langle\hat{I}_\alpha(t)\rangle$ to calculate the current fluctuation correlation function:

$$\langle \delta\hat{I}_\alpha(t)\,\delta\hat{I}_\alpha(0)\rangle = \frac{e^2}{h^2}\sum_{\rho\rho'} \sum_{\sigma\sigma'\sigma''\sigma'''} \sum_{\beta\gamma\delta\zeta} \int dE dE' dE'' dE'''$$

$$\times e^{i(E-E')t/\hbar} A^{\alpha\rho}_{\beta\gamma\sigma\sigma'} A^{\alpha\rho'}_{\delta\zeta\sigma''\sigma'''} \Delta^{\sigma\sigma'\sigma''\sigma'''}_{\beta\gamma\delta\zeta}, \tag{C4}$$

$$\Delta^{\sigma\sigma'\sigma''\sigma'''}_{\beta\gamma\delta\zeta} \equiv \langle \hat{a}^\dagger_{\beta\sigma}(E)\hat{a}_{\gamma\sigma'}(E')\hat{a}^\dagger_{\delta\sigma''}(E'')\hat{a}_{\zeta\sigma'''}(E''')\rangle - \langle \hat{a}^\dagger_{\beta\sigma}(E)\hat{a}_{\gamma\sigma'}(E')\rangle\langle \hat{a}^\dagger_{\delta\sigma''}(E'')\hat{a}_{\zeta\sigma'''}(E''')\rangle. \tag{C5}$$

Although we derived an expression for the current operator in the SO coupling basis, we choose here to express all of the operators in the standard spin basis,

$$\hat{a}^\dagger_{\beta\sigma}(E) = \frac{[e^{i\theta_\beta/2}\hat{a}^\dagger_{\beta\uparrow}(k(E,\sigma)) + \eta_\sigma e^{-i\theta_\beta/2}\hat{a}^\dagger_{\beta\downarrow}(k(E,\sigma))]}{\sqrt{2D_\sigma(k)}}, \tag{C6}$$

with $D_\sigma(k) \equiv dE(k,\sigma)/dk = \hbar^2 k/m + \eta_\sigma \alpha$. Defining $\Pi \equiv \sqrt{D_\sigma(k)D_{\sigma'}(k')D_{\sigma''}(k'')D_{\sigma'''}(k''')}$, we have

$$\begin{aligned}\Delta^{\sigma\sigma'\sigma''\sigma'''}_{\beta\gamma\delta\zeta} = \frac{1}{4\Pi}\{ & \delta_{\beta\zeta}\delta_{\gamma\delta}\delta(k_{E,\sigma} - k_{E''',\sigma'''})\,\delta(k_{E',\sigma'} \\ & - k_{E'',\sigma''})n_{\beta\uparrow}(k_{E,\sigma})[1 - n_{\gamma\uparrow}(k_{E',\sigma'})] + \cdots \\ & + \eta_{\sigma'}\eta_{\sigma''}\delta_{\beta\zeta}\delta_{\gamma\delta}\delta(k_{E,\sigma} - k_{E''',\sigma'''}) \\ & \times \delta(k_{E',\sigma'} - k_{E'',\sigma''})n_{\beta\uparrow}(k_{E,\sigma})\},\end{aligned} \tag{C7}$$

where $k_{E,\sigma} = k_{E',\sigma'}$ for $E = E' + \alpha k(\eta_{\sigma'} - \eta_\sigma)$, so that $\delta(k_{E,\sigma} - k_{E''',\sigma'''}) = D_\sigma(k)\,\delta[E - E''' + \alpha k(\eta_\sigma - \eta_{\sigma'''})]$. After integration over E'' and E''' and making the approximation $D_+(k) \approx D_-(k)$, we find

$$\begin{aligned}\int dE''dE'''\Delta^{\sigma\sigma'\sigma''\sigma'''}_{\beta\gamma\delta\zeta} & \\ = \tfrac{1}{4}[& \delta_{\beta\zeta}\delta_{\gamma\delta}n_{\beta\uparrow}(k_{E,\sigma})[1 - n_{\gamma\uparrow}(k_{E',\sigma'})] \\ & + \eta_{\sigma'}\eta_{\sigma''}\delta_{\gamma\delta}n_{\beta\uparrow}(k_{E,\sigma})].\end{aligned} \tag{C8}$$

We can replace $D_-(k)$ by $D_+(k)$, because

$$\frac{D_-(k)}{D_+(k)} = \frac{\dfrac{\hbar^2 k}{m} - \alpha}{\dfrac{\hbar^2 k}{m} + \alpha} \approx 1 + \frac{\alpha}{\dfrac{\hbar^2 k}{2m}} \approx 1,$$

which follows from

$$\frac{\alpha}{\dfrac{\hbar^2 k}{2m}} \leqslant \frac{\alpha k_f}{\left(\dfrac{\hbar^2 k_f^2}{2m}\right)} = \frac{E_{\mathrm{SO}}(k_f)}{E_c(k_f)} \ll 1$$

as the SO coupling is small. We will now calculate the power spectral density at zero frequency in output lead number 4, $S_{44}(0)$,

$$S_{44}(0) = \frac{e^2}{2h}\sum_{\rho\rho'}\sum_{\sigma\sigma'\sigma''\sigma'''}\sum_{\beta,\gamma=1,2} A^{4\rho}_{\beta\gamma\sigma\sigma'}A^{4\rho'}_{\gamma\beta\sigma''\sigma'''} \times \int dE n_{\beta\uparrow}(k_{E,\sigma})[1 - n_{\gamma\uparrow}(k_{E,\sigma'}) + \eta_{\sigma'}\eta_{\sigma''}], \tag{C9}$$

where $\gamma = 1$ or 2, since we have ignored the scattering from output lead to output lead. $n_{\beta\uparrow}(k_{E,\sigma})$ is the number of electrons in lead β with spin up and momentum $k_{E,\sigma}$,

$$n_{\beta\uparrow}(k_{E,\sigma}) = \begin{cases} 0 & \text{if } E \leqslant E_1 + \eta_\sigma \alpha k_1, \\ 1 & \text{if } E_1 + \eta_\sigma \alpha k_1 \leqslant E \leqslant E_2 + \eta_\sigma \alpha k_2, \\ 0 & \text{if } E_2 + \eta_\sigma \alpha k_2 \leqslant E. \end{cases}$$

Assuming that the SO coupling is weaker than the bias voltage, that is, $E_1 + \alpha k_1 \leqslant E_2 - \alpha k_2$, we have $n_{\beta\uparrow}(k_{E,-})[1 - n_{\gamma\uparrow}(k_{E,+})] \neq 0$ for $E_1 - \alpha k_1 \leqslant E \leqslant E_1 + \alpha k_1$ and $n_{\beta\uparrow}(k_{E,+})[1 - n_{\gamma\uparrow}(k_{E,-})] \neq 0$ for $E_2 - \alpha k_2 \leqslant E \leqslant E_2 + \alpha k_2$. Therefore, Eq. (C9) becomes

$$\begin{aligned}S_{44}(0) = \frac{e^2}{2h}\sum_{\rho\rho'}\sum_{\sigma\sigma'\sigma''\sigma'''}\sum_{\beta,\gamma} A^{4\rho}_{\beta\gamma\sigma\sigma'}A^{4\rho'}_{\gamma\beta\sigma''\sigma'''}[& \eta_{\sigma'}\eta_{\sigma''}e\Delta V \\ & + \delta_{\sigma+}\delta_{\sigma'-}2\alpha k_2 + \delta_{\sigma-}\delta_{\sigma'+}2\alpha k_1].\end{aligned} \tag{C10}$$

Given the scattering matrix calculated in Eq. (36), we find

$$\sum_{\rho\rho'}\sum_{\sigma\sigma'\sigma''\sigma'''}\sum_{\beta,\gamma} A^{4\rho}_{\beta\gamma\sigma\sigma'}A^{4\rho'}_{\gamma\beta\sigma''\sigma'''}\eta_{\sigma'}\eta_{\sigma''} = 0 \tag{C11}$$

and

$$\sum_{\rho\rho'}\sum_{\sigma\sigma'\sigma''\sigma'''}\sum_{\beta,\gamma} A^{4\rho}_{\beta\gamma\sigma\sigma'}A^{4\rho'}_{\gamma\beta\sigma''\sigma'''}\delta_{\sigma+}\delta_{\sigma'-} = 4TR\sin^2\theta, \tag{C12}$$

so that

$$S_{44}(0) = \frac{2e^2}{h}(2\alpha k_1 + 2\alpha k_2)T(1-T)\sin^2\theta. \tag{C13}$$

After some calculation, we find the current and Fano factor to be

$$\langle I_4 \rangle = \frac{e^2}{h}\Delta V, \tag{C14}$$

$$F \equiv \frac{S_{44}(0)}{2e\langle I_4\rangle} = 2T(1-T)\sin^2\theta\left[\frac{\alpha k_1 + \alpha k_2}{e\Delta V}\right]. \tag{C15}$$

This is identical to the the current and Fano factor shown in Eq. (51).

*Also at ENS Cachan, 61 avenue du president Wilson, 94235 Cachan Cedex, France.
†Also at NTT Basic Research Laboratories, 3-1 Morinosato-Wakamiya Atsugi, Kanagawa 243-01, Japan.
[1] K. von Klitzing, G. Dorda, and M. Pepper, Phys. Rev. Lett. **45**, 494 (1980).
[2] B. J. van Wees, H. van Houten, C. W. J. Beenakker, J. G. Williamson, L. P. Kouwenhoven, D. van der Marel, and C. T. Foxon, Phys. Rev. Lett. **60**, 848 (1988).
[3] D. A. Wharam, T. J. Thornton, R. Newbury, M. Pepper, H. Ahmed, J. E. F. Frost, D. G. Hasko, D. C. Peacock, D. A. Ritchie, and G. A. C. Jones, J. Phys. C **21**, L209 (1988).
[4] M. Henny, S. Oberholzer, C. Strunk, T. Heinzel, K. Ensslin, M. Holland, and C. Schönenberger, Science **284**, 296 (1999).
[5] W. D. Oliver, J. Kim, R. C. Liu, and Y. Yamamoto, Science **284**, 299 (1999).
[6] R. C. Liu, B. Odom, Y. Yamamoto, and S. Tarucha, Nature (London) **391**, 263 (1998).
[7] R. de-Picciotto, M. Reznikov, M. Heiblum, V. Umansky, G. Bunin, and D. Mahalu, Nature (London) **289**, 162 (1997).
[8] L. Saminadayar, D. C. Glattli, Y. Jin, and B. Etienne, Phys. Rev. Lett. **79**, 2526 (1997).
[9] G. Burkard, D. Loss, and E. V. Sukhorukov, Phys. Rev. B **61**, 16 303 (2000).
[10] X. Maître, W. D. Oliver, and Y. Yamamoto, Physica E (Amsterdam) **6**, 301 (2000).
[11] W. D. Oliver, R. C. Liu, J. Kim, X. Maître, L. Di Carlo, and Y. Yamamoto, in *Quantum Mesoscopic Phenomena and Mesoscopic Devices in Microelectronics*, edited by I. O. Kulik and R. Ellialtioğlu, Vol. 559 of *NATO Advanced Study Institute, Series C* (Kluwer, Dordrecht, 2000), pp. 457–466.
[12] R. Ionicioiu, P. Zanardi, and F. Rossi, Phys. Rev. A **63**, 050101(R) (2001).
[13] P. Recher, E. V. Sukhorukov, and D. Loss, Phys. Rev. B **63**, 165314 (2001).
[14] W. D. Oliver, F. Yamaguchi, and Y. Yamamoto, Phys. Rev. Lett. **88**, 037 901 (2002).
[15] M. Büttiker, Phys. Rev. B **46**, 12 485 (1992).
[16] T. Martin and R. Landauer, Phys. Rev. B **45**, 1742 (1992).
[17] G. Dresselhaus, Phys. Rev. **100**, 580 (1955).
[18] E. I. Rashba, Fiz. Tverd. Tela (Leningrad) **2**, 1224 (1960) [Sov. Phys. Solid State **2**, 1109 (1960)].
[19] Yu. A. Bychkov and E. I. Rashba, Pis'ma Zh. Éksp. Teor. Fiz. **39**, 66 (1984) [JETP Lett. **39**, 78 (1984)].
[20] S. Datta and B. Das, Appl. Phys. Lett. **56**, 665 (1990).
[21] F. Mireles and G. Kirczenow, Phys. Rev. B **64**, 024426 (2001).
[22] L. I. Schiff, *Quantum Mechanics* (McGraw-Hill, New-York, 1968).
[23] B. Das, S. Datta, and R. Reifenberger, Phys. Rev. B **41**, 8278 (1990).
[24] G. L. Chen, J. Han, T. T. Huang, S. Datta, and D. B. Janes, Phys. Rev. B **47**, 4084 (1993).
[25] J. Luo, H. Munekata, F. F. Fang, and P. J. Stiles, Phys. Rev. B **41**, 7685 (1990).
[26] F. J. Ohkawa and Y. Uemura, J. Phys. Soc. Jpn. **37**, 1325 (1974).
[27] T. Ando, A. B. Fowler, and F. Stern, Rev. Mod. Phys. **54**, 437 (1982).
[28] P. Pfeffer and W. Zawadzki, Phys. Rev. B **52**, 14 332 (1995).
[29] P. Pfeffer, Phys. Rev. B **55**, 7359 (1997).
[30] L. Wissinger, U. Rössler, R. Winkler, B. Jusserand, and D. Richards, Phys. Rev. B **58**, 15 375 (1998).
[31] P. Pfeffer, Phys. Rev. B **59**, 15 902 (1998).
[32] J. Nitta, T. Akazaki, H. Takayanagi, and T. Enoki, Phys. Rev. Lett. **78**, 1335 (1997).
[33] G. Engels, J. Lange, Th. Schäpers, and H. Lüth, Phys. Rev. B **55**, 1958 (1997).
[34] J. P. Heida, B. J. van Wees, J. J. Kuipers, T. M. Klapwijk, and G. Borghs, Phys. Rev. B **57**, 11 911 (1998).
[35] th. Schäpers, G. Engels, J. Lange, Th. Klocke, M. Hollfelder, and H. Lüth, J. Appl. Phys. **83**, 4324 (1998).
[36] C. M. Hu, J. Nitta, T. Akazaki, H. Takayanaga, J. Osaka, P. Pfeffer, and W. Zawadski, Phys. Rev. B **60**, 7736 (1999).
[37] D. Grundler, Phys. Rev. Lett. **84**, 6074 (2000).
[38] T. Matsuyama, R. Kürsten, C. Meissner, and U. Merkt, Phys. Rev. B **61**, 15 588 (2000).
[39] T. Hassenkam, S. Pedersen, K. Baklanov, A. Kristensen, C. B. Sorensen, P. E. Lindelof, F. G. Pikus, and G. E. Pikus, Phys. Rev. B **55**, 9298 (1997).
[40] A. V. Moroz and C. H. W. Barnes, Phys. Rev. B **60**, 14 272 (1999).
[41] Ya. M. Blanter and M. Büttiker, Phys. Rep. **336**, 1 (2000).
[42] J. C. Egues, G. Burkard, and D. Loss, cond-mat/0204639 (unpublished).